Elimination of thermoelectric artifacts in the harmonic Hall measurement of spin-orbit torque

Eun-Sang Park,[1,2] Dong-Kyu Lee,[3] Byoung-Chul Min,[2,4] and Kyung-Jin Lee[1,3,*]

[1]*KU-KIST Graduate School of Converging Science and Technology, Korea University, Seoul 02841, Korea*

[2]*Center for Spintronics, Korea Institute of Science and Technology, Seoul 02792, Korea*

[3]*Department of Materials Science and Engineering, Korea University, Seoul 02841, Korea*

[4]*Division of Nanotechnology and Information Technology, KIST School, Korea University of Science and Technology, Seoul 02792, Korea*

(Received 1 October 2018; revised manuscript received 18 November 2019; published 30 December 2019)

The harmonic Hall measurement is widely used to determine the equivalent field of current-induced spin-orbit torque in ferromagnet/normal metal bilayers. We report that this method suffers from various thermoelectric artifacts that have not been considered. We propose and experimentally demonstrate how to eliminate major thermoelectric artifacts using, namely, the four-direction (4-D) methods interchanging current and field polarities, which allow us to determine the magnitudes and angular dependences of spin-orbit torques more accurately than a conventional method. The proposed 4-D method will be useful for searching suitable materials for device applications operated by spin-orbit torques.

DOI: 10.1103/PhysRevB.100.214438

I. INTRODUCTION

The recent discovery of spin-orbit torque (SOT) in ferromagnet/normal metal bilayers opens a new route to control the magnetization [1,2]. The SOT is a torque exerting on a magnetic layer by a perpendicular spin current converted from an in-plane charge current through the spin-orbit coupling thereby offering a write scheme for three-terminal spintronic devices operated by an in-plane charge current. The use of an in-plane current provides various advantages as compared to the use of a perpendicular charge current that is essential for the writing scheme based on conventional spin-transfer torques [3]. The SOT allows deterministic switching of an in-plane magnetization [2] as well as a perpendicular magnetization (when an external or effective field is applied [1,4–9] or the spin current carries the out-of-plane spin polarization [10–12]). It also efficiently moves ferromagnetic [13–15] and ferrimagnetic [16–18] domain walls and skyrmions [19–22]. Because of this widespread applicability, the SOT study has become an important research field in the spintronics.

For the SOT studies and SOT-active device applications, it is important to accurately quantify the SOT or the spin Hall angle, the ratio of a spin current density to a charge current density. Several methods have been proposed and used; including the spin-torque ferromagnetic resonance [23], the harmonic Hall voltage measurement [24–27], the domain-wall measurement [28], the magneto-optical Kerr measurement [29], and the current-induced hysteresis loop shift [30]. Among them, the harmonic Hall method is most widely used because it allows to separately quantify two mutually orthogonal components of SOT, i.e., dampinglike and fieldlike ones [25], and their angular dependences [26]. Separate determination of dampinglike and fieldlike SOTs is important because not only the dampinglike torque, but also the fieldlike torque is crucial for magnetization switching dynamics [31–37]. It is also important to measure the angular dependence of SOT as it provides a clue for the microscopic mechanism of SOT [38] and affects the SOT efficiencies [39]. Although it is widely used, the accuracy of this method is known to be influenced by several effects, such as the anomalous Nernst effect [26] or higher-order anisotropy [40]. Therefore, a careful elimination of signals unrelated to the SOT in the harmonic Hall measurement is essential to characterize the SOT.

The Hall voltage measurement usually contains several artifacts originating from the thermoelectric effect because an electrical current injected into a Hall bar structure generates a temperature gradient in an uncontrollable way [41]. Possible sources of such a temperature gradient include current-induced Joule heating and Peltier effects. It is usually uneasy to experimentally measure temperature gradients caused by Joule heating or the Peltier effect.

For determining the SOT, both first- and second-harmonic signals with respect to an ac current must be measured as the first-harmonic signal gives information of the equilibrium magnetization direction whereas the second-harmonic signal describes a SOT-induced small tilting of magnetization from the equilibrium direction. For the conventional Hall measurement where no SOT contribution is involved, a way to eliminate these artifacts from the first-harmonic Hall signal is to use the sign dependence of Hall and thermoelectric effects with respect to the directions of current and magnetic field [41]. In this paper, we expand this method to the second-harmonic Hall signal, directly related to the SOT, and show that some thermoelectric artifacts can be properly eliminated using so-called four-direction (4-D) method explained below.

II. THERMOELECTRIC ARTIFACTS IN THE HARMONIC HALL VOLTAGES

We first discuss thermoelectric artifacts in the conventional Hall voltages in which no SOT contribution is involved.

*Corresponding author: kj_lee@korea.ac.kr

TABLE I. The signs of the current and the field for four first-harmonic voltages ($V_1^{1\omega}$, $V_2^{1\omega}$, $V_3^{1\omega}$, and $V_4^{1\omega}$). Corresponding signs of Hall voltage (V_H) and other thermoelectric voltages.

	Current	Field	Hall	Thermoelectric artifacts				
V_H^{1w}	I	B	V_H	V_N	V_S	V_E	V_R	V_O
$V_1^{1\omega}$	+	+	+	+	+	+	+	+
$V_2^{1\omega}$	−	+	−	+	+	−	+	+
$V_3^{1\omega}$	+	−	−	−	+	−	−	+
$V_4^{1\omega}$	−	−	+	−	+	+	−	+

It is known that a normal (first-harmonic) Hall voltage (V_H) contains several artifacts, such as Seebeck (V_S), Nernst (V_N), Ettingshaussen (V_E), Righi-Leduc effects (V_R), as well as misalignment (V_M) and Ohmic offset (V_O) [41]. These artifacts can be eliminated by considering the current and magnetic-field symmetry because each voltage has a different sign dependence on the current and field directions as summarized in Table I. For example, the Seebeck signal (V_S) does not depend on the sign of current or field whereas the sign of the Nernst signal (V_N) follows the sign of field. Among the artifacts, V_N, V_E, and V_R are artifacts influenced by the vertical component of the external magnetic-field (H_z) and magnetization (M_z). When we apply in-plane magnetic-fields (H_x or H_y) to perpendicularly magnetized samples, the magnetization is tilted toward the magnetic fields but does not fully align with the magnetic field. The essence of the proposed method relies on the sign dependence of an artifact with respect to the signs of current and magnetization because some artifacts are eliminated by adding or subtracting four harmonic signals obtained from different polarities of current and magnetization. Reversing the direction of external field accordingly reverses the direction of magnetization as well. In this respect, the overall sign, not the exact direction, of magnetization is important, and, thus, the misalignment between the magnetic field and the magnetization does not alter the main conclusion of this paper. This argument does not work for small field ranges where the second harmonic signals exhibit a hysteresis loop. As we will show below, however, artifacts related to the hysteresis loop can be eliminated in our method.

We determine the anomalous Hall voltage (V_{AH}) with changing the polarities of the current and the magnetic field. The signs of current and field corresponding to $V_i^{1\omega}$ ($i = 1$–4) are given in Table I. We note that, in ferromagnets, the Hall (V_H) and Nernst (V_N) signals are accompanied by the anomalous Hall (V_{AH}) and anomalous Nernst signal (V_{ANE}). Using the sign dependence of thermoelectric artifacts in Table I, one finds the following relation for four Hall voltages measured with four different sign combinations of the current and field,

$$V_1^{1\omega} - V_2^{1\omega} - V_3^{1\omega} + V_4^{1\omega} = 4V_{AH} + 4V_H + 4V_E. \quad (1)$$

Equation (1) allows us to determine V_{AH} as V_H can be readily subtracted, and V_E is usually negligible [41].

The above-listed thermoelectric voltages also affect the second-harmonic Hall voltage that determines SOT. For a coordinate system shown in Fig. 1(a), the SOT, $\mathbf{N}_{\mathrm{SOT}}$ is described as

$$\mathbf{N}_{\mathrm{SOT}} = a\,\mathbf{M} \times (\mathbf{M} \times \mathbf{y}) + b(\mathbf{M} \times \mathbf{y}), \quad (2)$$

where $\mathbf{M}$ is the unit vector along the magnetization, $\mathbf{y}$ is the unit vector perpendicular to both directions of the current-flow direction (x) and film normal (z), and coefficients a and b are the magnitudes of dampinglike torque (DLT) and fieldlike torque (FLT), respectively. Two independent measurements with different field angles are required to measure a and b [25]; the DLT (FLT) component a (b) is measured with an external field H_{ext} applied in the x direction (y direction). The second-harmonic voltage changes its sign depending on the field sign due to the symmetry given in Eq. (2). The directions of DLT and FLT effective fields are in the directions along ($\mathbf{M} \times \mathbf{y}$) and $\mathbf{y}$, respectively. Therefore, when the field direction is reversed (i.e., $\mathbf{M}$ is reversed accordingly), the second-harmonic signal for the dampinglike component (V_{DLT}) changes its sign whereas that for the fieldlike component (V_{FLT}) does not change. As a result, one can construct the sign relation of the second-harmonic signal with respect to the signs of current and field for DLT and FLT configurations (see Table II). In Appendix A, we summarize explicit functional forms of electric Hall voltages (i.e., anomalous Hall and planar Hall voltages) and electric longitudinal voltage originating from a misalignment of Hall cross area. In Appendix B, we summarize explicit functional forms of established thermoelectric effects (i.e., anomalous Nernst effect and planar Nernst effect). In Appendix C, we present macrospin simulation results for artifacts originating from the

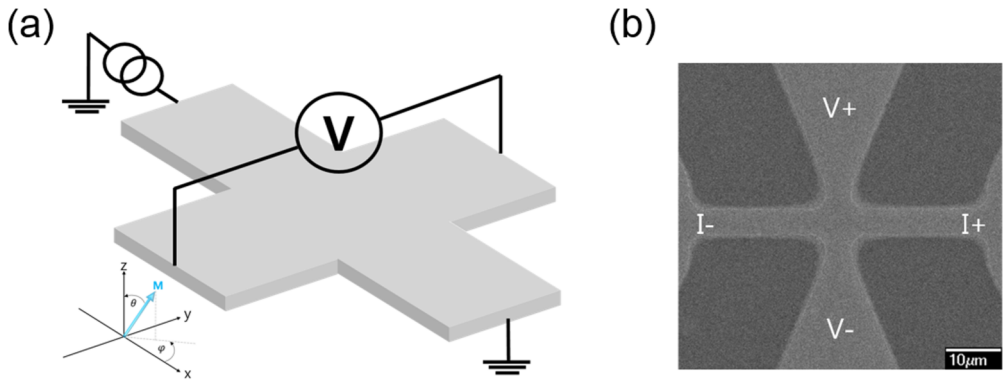

FIG. 1. (a) A schematic of the device geometry and the coordinate system. (b) A scanning electron microscopy image of the Hall device.

TABLE II. The signs of the current and the field for four second-harmonic voltages ($V_1^{2\omega}, V_2^{2\omega}, V_3^{2\omega}$, and $V_4^{2\omega}$). Corresponding signs of Hall voltages for the DLT ($V_{\rm DLT}$) geometry, FLT ($V_{\rm FLT}$) geometry, and other thermoelectric effects.

	Current	Field	$H_{\rm ext} \parallel x$	$H_{\rm ext} \parallel y$	Thermoelectric artifacts				
V_H^{2w}	I	B	$V_{\rm DLT}$	$V_{\rm FLT}$	V_N	V_S	V_E	V_R	V_O
$V_1^{2\omega}$	+	+	+	+	+	+	+	+	+
$V_2^{2\omega}$	−	+	+	+	−	+	−	+	+
$V_3^{2\omega}$	+	−	−	+	−	+	−	−	+
$V_4^{2\omega}$	−	−	−	+	+	+	+	−	+

misalignment and thermoelectric effects and discuss which artifacts are eliminated in our 4-D method and which are not.

We determine the magnitude of SOTs with changing the polarities of the current and magnetic field. From Table II, we find the following relations:

$$\text{DLT geometry } (H_{\rm ext} \parallel x): V_1^{2\omega} + V_2^{2\omega} - V_3^{2\omega} - V_4^{2\omega} = 4V_{\rm DLT} + 4V_R, \quad (3)$$

$$\text{FLT geometry } (H_{\rm ext} \parallel y): V_1^{2\omega} + V_2^{2\omega} + V_3^{2\omega} + V_4^{2\omega} = 4V_{\rm FLT} + 4V_S + 4V_O. \quad (4)$$

Using Eq. (3), one can determine $V_{\rm DLT}$ because the Righi-Leduc signal (V_R) is the second-order effect of a thermal current and, thus, negligible. Using Eq. (4), one can determine $V_{\rm FLT}$ because the Seebeck signal (V_S) and Ohmic offset (V_O) give a constant offset to the second-harmonic signals as we will show in Sec. III.

III. EXPERIMENTAL RESULTS

We prepared two types of sample, Ta (5 nm)/ Pt (3 nm)/ Co (0.6 nm)/ MgO (2 nm)/ Ta (2 nm) and Ta (5 nm)/ $Co_4Fe_4B_2$ (1 nm)/ MgO (2 nm)/ Ta (2 nm) using the magnetron sputtering system at a base pressure of low 10^{-8} Torr. We deposit Ta and Pt layers at an Ar pressure of 3 mTorr, Co and CoFeB layers at 1 mTorr, and a MgO layer at 4 mTorr. The equilibrium magnetization direction of Co or the CoFeB layer is perpendicular to the film plane because it is thin. We then patterned the samples into Hall bars (Hall cross area of $5 \times 5\,\mu m^2$) by ion milling and photolithography. We measure the first- and second-harmonic signals as a function of magnetic field in DLT and FLT geometries with a lock-in amplifier. We changed the current sign by interchanging the current probes while keeping the voltage probe contacts unchanged (see Appendix D for details on changing the current direction).

We first measured harmonic Hall voltages for Ta/Pt/Co/MgO structure. Figure 2(a) shows magnetic-field-dependent first harmonic signal V_H^{1w} at ac currents of +1.5 and of −1.5 mA, respectively. With increasing the field, the magnetization of Co is tilted from the film normal to the plane. As a result, the absolute value of V_H^{1w}, mainly governed by the anomalous Hall effect (AHE) of a Co layer, gradually decreases with increasing the field. On top of this AHE-related signal, we also observe a large offset whose sign depends on the current sign. Figure 2(b) shows the corrected first-harmonic signal obtained from the average of four signals ($V_1^{1\omega}, V_2^{1\omega}, V_3^{1\omega}$, and $V_4^{1\omega}$ defined in Table I) according to Eq. (1). The corrected first-harmonic signal does not involve the current-dependent offset shown in Fig. 2(a). As explained for Eq. (1), V_E would still remain in the corrected signal but is presumed to be small because the Ettingshaussen effect is much smaller than the AHE.

Figure 3 shows the results of the second-harmonic signal V_H^{2w} for the DLT geometry ($H_{\rm ext} \parallel x$). We observe the hysteresis loop near the zero field for both current polarities [Fig. 3(a)]. This hysteresis loop is consistent with that expected from the anomalous Nernst effect (ANE) as already addressed in Ref. [26]. On top of this ANE-induced hysteresis, we observe that the slope of V_H^{2w} with respect to the external field is slightly different for ac currents with different polarities. This difference indicates that thermoelectric artifacts are involved in V_H^{2w} data measured for a given current and polarity. Figure 3(b) shows the corrected second-harmonic signal obtained from the average of four

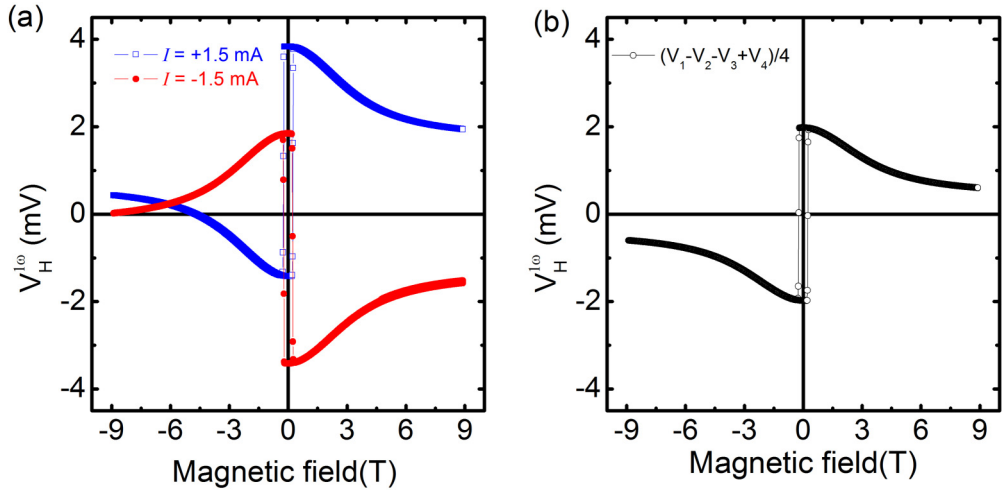

FIG. 2. Ta/Pt/Co/MgO structure: (a) Raw first-harmonic voltages ($V_H^{1\omega}$) versus the external magnetic field at injected ac currents of $I = +1.5$ and of $I = -1.5$ mA. (b) Corrected first-harmonic voltages using Eq. (1).

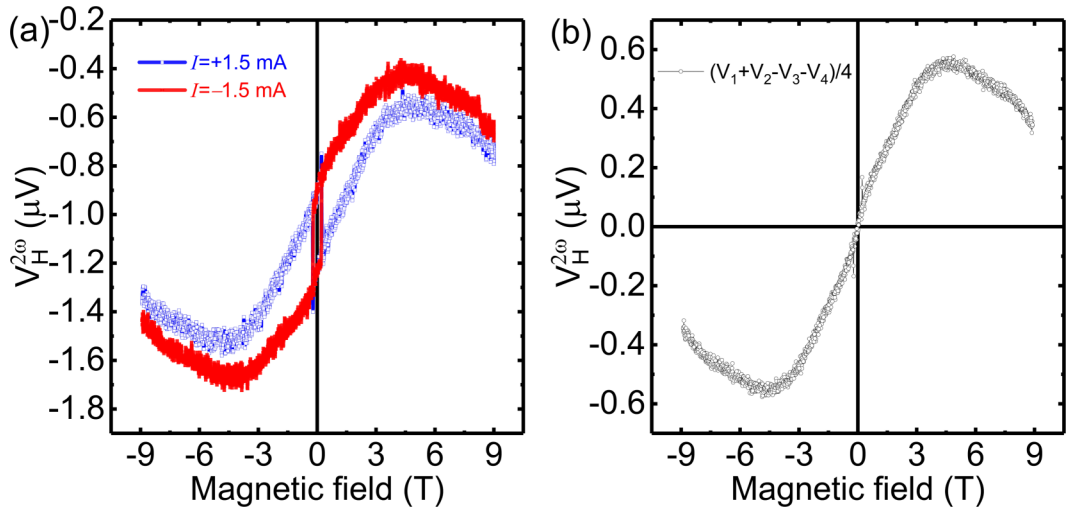

FIG. 3. Ta/Pt/Co/MgO structure: The second-harmonic signals for the DLT geometry ($B_{\text{ext}} \parallel x$). (a) Raw second-harmonic voltages ($V_H^{2\omega}$) versus the external magnetic field at injected ac currents of $I = +1.5$ mA and of $I = -1.5$ mA. (b) Corrected second-harmonic voltages using Eq. (3).

signals ($V_1^{2\omega}, V_2^{2\omega}$, $V_3^{2\omega}$, and $V_4^{2\omega}$ defined in Table II) according to Eq. (3). The corrected second-harmonic signal does not involve the ANE-induced hysteresis. According to Eq. (3), thermoelectric artifacts other than V_R are also eliminated in the data of Fig. 3(b). Given that the Righi-Leduc effect is usually much smaller than the AHE, we conclude that this method is largely free from thermoelectric artifacts.

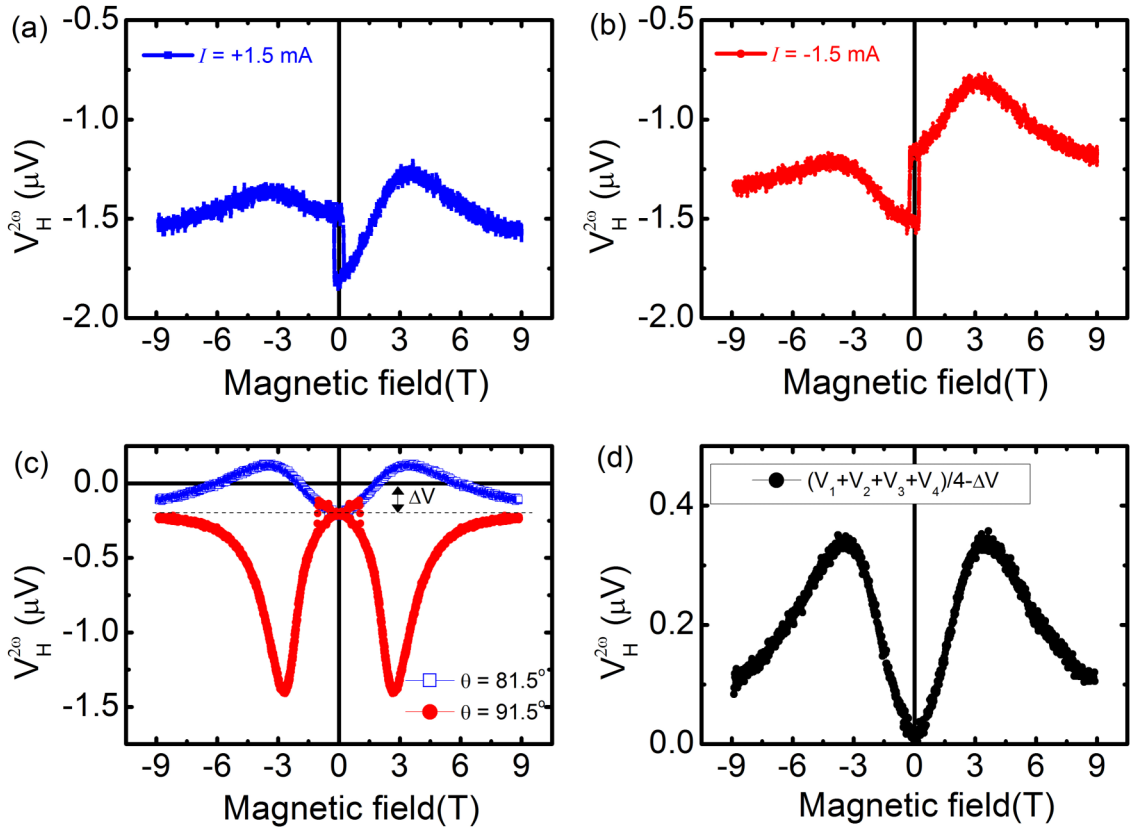

FIG. 4. Ta/Pt/Co/MgO structure: The second-harmonic signals for the FLT geometry ($B_{\text{ext}} \parallel y$). Raw second-harmonic voltages ($V_H^{2\omega}$) versus the external magnetic field at an injected ac current of (a) $I = +1.5$ mA and of (b) $I = -1.5$ mA. (c) Corrected second-harmonic voltages using Eq. (4). Here, the blue symbols are obtained from the field (polar) angle of 81.5°, whereas the red symbols are obtained from the field (polar) angle of 91.5°. A constant offset ΔV is indicated. (d) Fully corrected second-harmonic voltages by subtracting ΔV from the results shown in (c) (field angle = 81.5°).

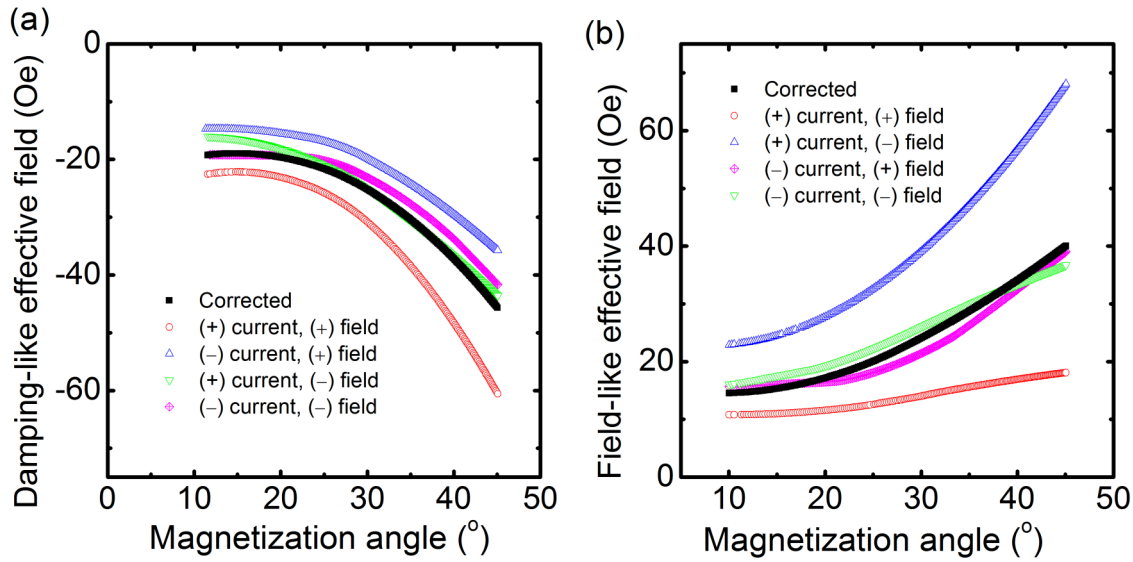

FIG. 5. Ta/Pt/Co/MgO structure: Angular dependence of (a) dampinglike and (b) fieldlike SOT effective fields. For each panel, one corrected and four uncorrected data are compared.

Figure 4 shows the second-harmonic signals for the FLT geometry ($H_{\text{ext}} \parallel y$). The ANE-induced hysteresis loops are also observed [Figs. 4(a) and 4(b)]. On top of this hysteresis, we observe a large offset that is dependent on the current polarity. We also observe that the slope of V_H^{2w} with respect to the external field is apparently different for the signs of current and field. The blue symbols in Fig. 4(c) are the corrected second-harmonic signals obtained from the average of four signals ($V_1^{2\omega}$, $V_2^{2\omega}$, $V_3^{2\omega}$, and $V_4^{2\omega}$ defined in Table II) according to Eq. (4). The corrected second-harmonic signal does not involve the ANE-induced hysteresis but shows an offset indicated by ΔV. According to Eq. (4), the corrected second-harmonic signals for the FLT geometry contain Seebeck signal (V_S) and Ohmic offset (V_O). To check whether or not ΔV is dependent on the magnetization direction, we repeated the same second-harmonic Hall measurements for the FLT geometry with a different field angle. In Fig. 4(c), the blue symbols are obtained from the field (polar) angle of 81.5° whereas the red symbols are obtained from the field (polar) angle of 91.5°. They show V_H^{2w} of the opposite signs because out-of-plane components of the field are the opposite in these two cases. The magnitudes of V_H^{2w} are also different because the field angles measured from the film plane are different (8.5° for the former and −1.5° for the latter). We observe, however, that the offset ΔV is independent of the field angle, meaning that ΔV is unrelated to the magnetization oscillation driven by SOT. Therefore, we subtract this ΔV from the corrected signal to obtain V_H^{2w} relevant to SOT [Fig. 4(d)].

Results in Figs. 3 and 4 show that thermoelectric artifacts in V_H^{2w} are non-negligible. In order to directly demonstrate their effects on the estimation of SOT, we calculate dampinglike [Fig. 5(a)] and fieldlike [Fig. 5(b)] effective fields from the corrected V_H^{1w} and V_H^{2w}, following the procedure in Ref. [26] with considering the planar Hall effect and the field angle. For comparison, we also include dampinglike and fieldlike effective fields calculated from uncorrected V_H^{1w} and V_H^{2w} for a given current polarity. We remove a constant offset and ANE for the uncorrected data as performed in Ref. [26]. The effective fields for the polar angle of magnetization larger than 10° are shown because the second-harmonic Hall signals are too noisy to get meaningful values for the angle below 10°. We find that the uncorrected harmonic signals give apparently different SOT effective fields from the corrected ones not only in the magnitude, but also in the angular dependence. For the sample we measure, the largest difference of SOT effective fields reaches about 100%, thus, a difference by a factor of 2. These values mean that we should consider thermal artifacts. Otherwise, the final results with thermal artifacts will be over- or underestimated.

We also apply the 4-D method to another structure Ta/CoFeB/MgO to check whether or not the large artifacts observed in the Pt/Co/MgO trilayer is specific to a structure. As shown in Fig. 6, the asymmetry of the second-harmonic signals in the Ta/CoFeB/MgO structure is also visible, which eventually affects the evaluation of the effective SOT field. Therefore, the asymmetry is not specific to a structure but can appear in any Hall bar measurements.

IV. SUMMARY

In this paper, we propose the four-direction measurement that shows an improved accuracy for the estimation of the dampinglike and fieldlike SOTs. This improvement is caused by the fact that a nominally measured Hall signal can be influenced by thermoelectric effects and misalignment of the Hall cross. It turns out that the second-harmonic signals corresponding to the SOT are affected by these artifacts. We have shown that those effects, which deteriorate a correct Hall measurement of SOT, can be, at least, partially eliminated by considering the current and field symmetry. The elimination of artifacts provides an improved estimation the magnitude and angular dependence of SOT. Our result shows that a careful elimination of signals unrelated to the SOT in the harmonic Hall measurement is essential to characterize the SOT.

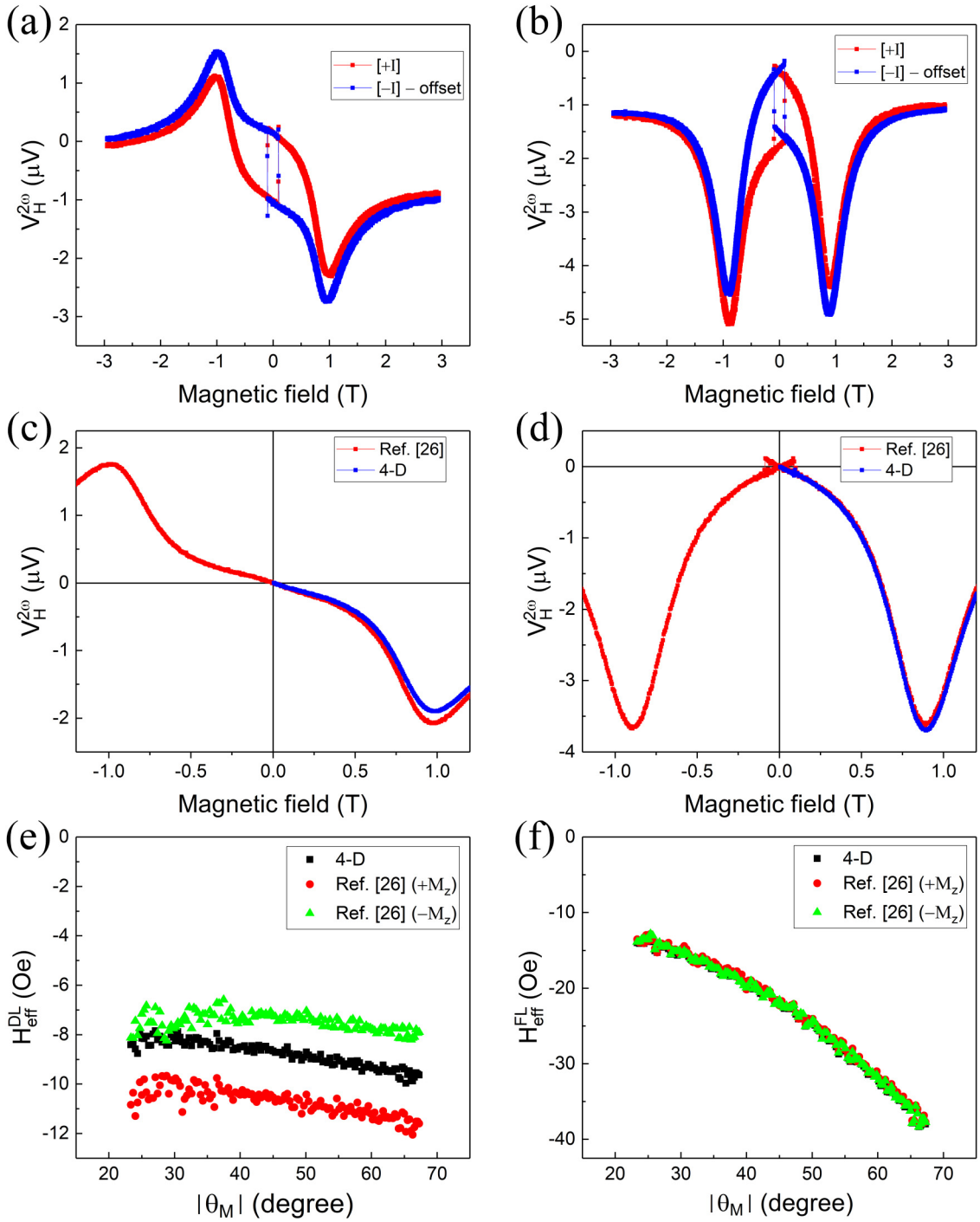

FIG. 6. Comparison of the 4-D measurement and conventional measurement (Ref. [26]) for a Ta/CoFeB/MgO structure. Raw second-harmonic signals for (a) the DLT geometry and (b) FLT geometry. (c) Uncorrected $V_H^{2\omega}$ (red symbols) that only ANE is removed and corrected $V_H^{2\omega}$ (blue symbols) using $\frac{(V_1^{2\omega}+V_2^{2\omega}-V_3^{2\omega}-V_4^{2\omega})}{4} = V_{\mathrm{DLT}} + V_R$ for $\varphi = 0^\circ$. (d) Uncorrected $V_H^{2\omega}$ (red symbols) that only ANE is removed and corrected $V_H^{2\omega}$ (blue symbols) using $\frac{V_1^{2\omega}+V_2^{2\omega}+V_3^{2\omega}+V_4^{2\omega}}{4} = V_{\mathrm{FLT}} + V_S + V_O$ for $\varphi = 90^\circ$. Angular dependence of (e) dampinglike and (f) fieldlike SOT effective fields. For each panel, one corrected (black symbols) and two uncorrected data are compared. The red symbols are obtained from $+M_z$ data (positive magnetic-field region) and green symbols are obtained from $-M_z$ data (negative magnetic-field region).

ACKNOWLEDGMENTS

This work was supported by the KIST Institutional Program (Project No. 2V05750) and the National Research Foundation of Korea (NRF) (Grants No. 2015M3D1A1070465 and No. 2017R1A2B2006119).

APPENDIX A: HARMONIC HALL VOLTAGE

When a current flows in the x direction in a structure with magnetization, the voltage in the y direction can arise due to the AHE and the planar Hall effect (PHE). These two effects are defined as

$$\boldsymbol{V}_{AH} = R_{AH}\,\boldsymbol{m}\times\boldsymbol{J}, \tag{A1}$$

$$\boldsymbol{V}_{PH} = R_{PH}\boldsymbol{m}\cdot(\boldsymbol{J}\cdot\boldsymbol{m}), \tag{A2}$$

where $\boldsymbol{m} = (m_x,\ m_y,\ m_z)$ is the unit vector along the magnetization, $\boldsymbol{J} = (J_0,\ 0,\ 0)$ is the electric current, R_{AH} is the AHE resistance, and R_{PH} is the PHE resistance. The net voltage is expressed as the sum of the two voltages,

$$\boldsymbol{V}_{\text{net}} = \boldsymbol{V}_{AH} + \boldsymbol{V}_{PH} = J_0\big(R_{PH}m_x^2,\ R_{AH}m_z + R_{PH}m_xm_y, - R_{AH}m_y + R_{PH}m_xm_z\big). \tag{A3}$$

Each component of Eq. (A3) describes three vector components of the induced net voltage: a longitudinal voltage generated in the current direction (V_{xx}), a Hall voltage generated in the transverse direction to the current (V_{xy}), and a voltage generated in the normal direction to current (V_{xz}). We note that when the Hall cross or Hall voltage contacts are misaligned, the second-harmonic Hall voltage (V_H) measures not only V_{xy}, but also V_{xx}, which is usually uncontrollable in experiment and, thus, is a source of artifacts. In this case, the actual voltage measured across the Hall cross is the sum of the first and second components of Eq. (A3),

$$V_{\text{meas}} = J_0\big[(R_{AH}m_z + R_{PH}m_xm_y) + \xi\big(R_{PH}m_x^2\big)\big], \tag{A4}$$

where ξ describes the degree of misalignment, which may vary from sample to sample.

When an ac current flows in the x direction, the magnetization oscillates around its equilibrium direction and is described as $\delta\boldsymbol{m} = J_0(\delta m_x,\ \delta m_y,\ \delta m_z)$. Replacing $\boldsymbol{m}$ to $\boldsymbol{m} + \delta\boldsymbol{m}$ in Eqs. (A1) and (A2), we obtain

$$\begin{aligned} V_{\text{meas}} = J_0\big[&\big(R_{AH}m_z^0 + R_{PH}m_x^0m_y^0\big) + \xi R_{PH}\big(m_x^0\big)^2\big] \\ &+ J_0^2\big[R_{AH}\delta m_z + R_{PH}\big(\delta m_ym_x^0 + \delta m_xm_y^0\big) \\ &+ 2\xi R_{PH}\delta m_xm_x^0\big], \end{aligned} \tag{A5}$$

where m_i^0 is the ith component of the equilibrium magnetization. In Eq. (A5), the first term (proportional to J_0) is the first-harmonic voltage $V_H^{1\omega}$ and the second term (proportional to J_0^2) is the second-harmonic voltage $V_H^{2\omega}$. The second-harmonic voltage can be further separated for the field geometry: DLT and FLT geometries, given as

$$V_{\text{meas}}^{1\omega} = J_0\big[\big(R_{AH}m_z^0 + R_{PH}m_x^0m_y^0\big) + \xi R_{PH}\big(m_x^0\big)^2\big], \tag{A6}$$

$$V_{\text{meas}}^{2\omega,\ \text{DLT}} = J_0^2\big[\big(R_{AH}\delta m_z + R_{PH}\delta m_ym_x^0\big) + 2\xi\big(R_{PH}\delta m_xm_x^0\big)\big], \tag{A7}$$

$$V_{\text{meas}}^{2\omega,\ \text{FLT}} = J_0^2\big[R_{AH}\delta m_z + R_{PH}\delta m_xm_y^0\big]. \tag{A8}$$

APPENDIX B: THERMOELECTRIC HALL VOLTAGE

When the system has a temperature gradient ($\boldsymbol{\nabla T}$), the thermoelectric effect can occur. Here, we summarize how thermoelectric effects affect the Hall voltage in the presence of the ANE and PNE.

We assume that the temperature has a gradient in the x and z directions. We also assume that the magnitude of the temperature gradient is proportional to J_0^1 (i.e., Peltier or Thomson effect) or J_0^2 (i.e., Joule heating). With these assumptions, we define $\boldsymbol{\nabla T}$ as

$$\boldsymbol{\nabla T} = \big(T_{x1}J_0 + T_{x2}J_0^2,\ 0,\ T_{z1}J_0 + T_{z2}J_0^2\big), \tag{B1}$$

where T_{ik} means a temperature gradient coefficient which is settled in the i direction and is proportional to J_0^k. $\boldsymbol{\nabla T}$ can be coupled with the magnetization, creating a voltage through as ANE and PNE, given as

$$\boldsymbol{V}_{AN} = R_{AN}\boldsymbol{m}\times\boldsymbol{\nabla T}, \tag{B2}$$

$$\boldsymbol{V}_{PN} = R_{PH}(\boldsymbol{m}\cdot\boldsymbol{\nabla T})\boldsymbol{m}, \tag{B3}$$

$$\boldsymbol{V}_{\text{total}}^{\text{thermo}} = \boldsymbol{V}_{AN} + \boldsymbol{V}_{PN}, \tag{B4}$$

where R_{AN} is the ANE resistance and R_{PN} is the PNE resistance. Following the same procedure in Appendix A, we obtain

$$V_{\text{total}}^{\text{thermo}} = V_{xy}^{\text{thermo}} + \xi V_{xx}^{\text{thermo}}, \tag{B5}$$

$$V_{xy}^{\text{thermo}} = (R_{AN}m_z + R_{PN}m_xm_y)\big(T_{x1}J_0 + T_{x2}J_0^2\big) + (R_{PN}m_ym_z - \rho_{AN}m_x)\big(T_{z1}J_0 + T_{z2}J_0^2\big), \tag{B6}$$

$$V_{xx}^{\text{thermo}} = \big(R_{PH}m_x^2\big)\big(T_{x1}J_0 + T_{x2}J_0^2\big) + (R_{AH}m_y + R_{PN}m_xm_z)\big(T_{z1}J_0 + T_{z2}J_0^2\big). \tag{B7}$$

From Eqs. (B5)–(B7), we obtain the first-harmonic and second-harmonic voltages of the thermoelectric effect. Assuming that the thermoelectric effect on $V_{\text{meas}}^{1\omega}$ is negligible, the contributions of the thermoelectric effects to the second-harmonic voltage are given as

$$\begin{aligned} V_{2\omega,\ total}^{\text{thermo}} = {}& V_{2\omega}^{\text{thermo}}(T_{x1}) + V_{2\omega}^{\text{thermo}}(T_{x2}) \\ &+ V_{2\omega}^{\text{thermo}}(T_{z1}) + V_{2\omega}^{\text{thermo}}(T_{z2}), \end{aligned} \tag{B8}$$

$$V_{2\omega}^{\text{thermo}}(T_{x1}) = J_0^2T_{x1}\begin{bmatrix} R_{AN}\delta m_z + R_{PN}\big(\delta m_ym_x^0 + \delta m_xm_y^0\big) \\ +2\xi\big(R_{PN}\delta m_xm_x^0\big)\end{bmatrix}, \tag{B9}$$

$$V_{2\omega}^{\text{thermo}}(T_{x2}) = J_0^2T_{x2}\big[R_{AN}m_z^0 + R_{PN}m_x^0m_y^0 + \xi R_{PN}\big(m_x^0\big)^2\big], \tag{B10}$$

$$V_{2\omega}^{\text{thermo}}(T_{z1}) = J_0^2T_{z1}\begin{bmatrix} -R_{AN}\delta m_x + R_{PN}\big(\delta m_zm_y^0 + \delta m_ym_z^0\big) \\ +2\xi\big[R_{AN}\delta m_y + R_{PN}\big(\delta m_zm_x^0 + \delta m_xm_z^0\big)\big]\end{bmatrix}, \tag{B11}$$

$$\begin{aligned} V_{2\omega}^{\text{thermo}}(T_{z2}) = J_0^2T_{z2}\big[&\big(-R_{AN}m_x^0 + R_{PN}m_y^0m_z^0\big) \\ &+ \xi\big(R_{AN}m_y^0 + R_{PN}m_x^0m_z^0\big)\big]. \end{aligned} \tag{B12}$$

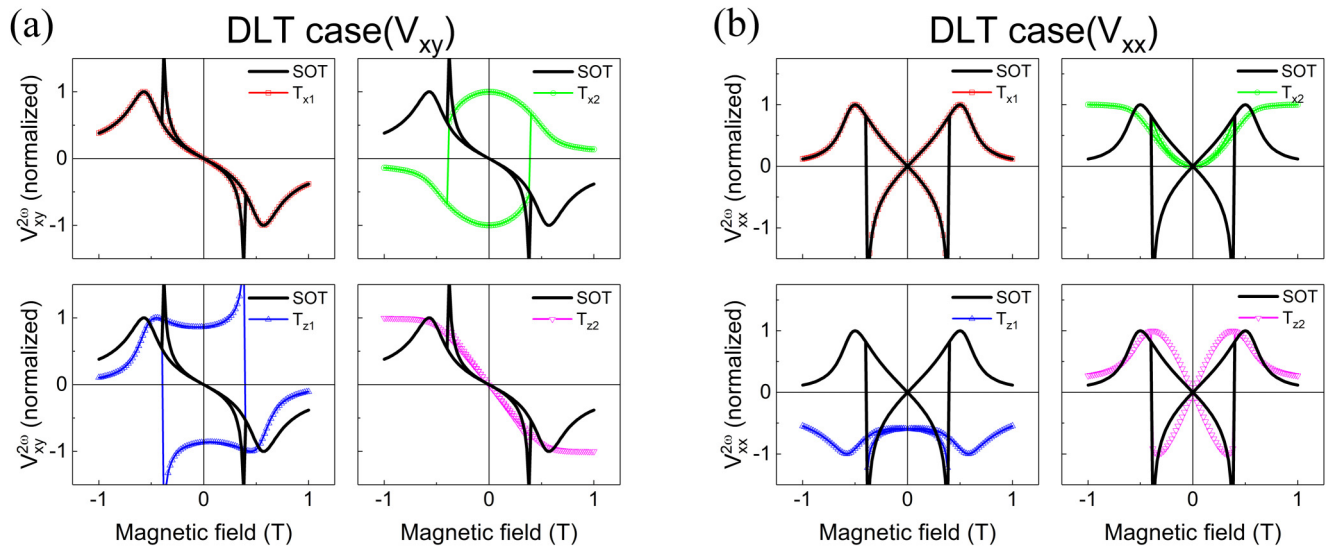

FIG. 7. Macrospin simulation of the second-harmonic signals induced by dampinglike SOT (DLT: black curve) and other thermoelectric effects (red, green, blue, and magenta symbols). (a) Hall voltage (V_{xy}) and (b) longitudinal voltage (V_{xx}), which contaminates the Hall signal due to the misalignment. T_{ik} means a temperature gradient in the i direction, induced by the kth order of an injected ac current.

APPENDIX C: MACROSPIN SIMULATION

We carry out macrospin simulation based on the Landau-Lifshitz-Gilbert equation including DLT and FLT,

$$\dot{\boldsymbol{m}} = -\gamma \boldsymbol{m} \times \boldsymbol{H} + \alpha \boldsymbol{m} \times \dot{\boldsymbol{m}} + \gamma c_{j,\mathrm{FLT}} \boldsymbol{m} \times \hat{\boldsymbol{y}} + \gamma c_{j,\mathrm{DLT}} \boldsymbol{m} \times (\boldsymbol{m} \times \hat{\boldsymbol{y}}), \tag{C1}$$

where $c_{j,\mathrm{FLT(DLT)}} = \frac{\hbar \theta_{\mathrm{FLT(DLT)}} J}{2eM_s t_z}$, $\theta_{\mathrm{FLT(DLT)}}$ is the effective spin Hall angle for FLT (DLT), $J = J_0 + T_{ik} J_0^k$, M_s is the saturation magnetization, and t_z is the thickness of ferromagnetic layer. The following parameters are used; $M_s = 1000$ emu/cm^3, $\gamma = 1.76 \times 10^7$ (Oe s)$^{-1}$, the perpendicular anisotropy field $H_K = 5000$ Oe, the Gilbert damping $\alpha = 0.1$, $\theta_{\mathrm{FLT}} = 0.1$, $\theta_{\mathrm{DLT}} = 0.1$, the polar angle of the applied magnetic-field $\theta_H = 86°$, $T_{ik} = 0.3$, and $J_0 = 1 \times 10^7 \mathrm{A/cm}^2$.

The simulation results are summarized in Figs. 7 and 8. From these results, one identifies which artifacts are eliminated but which are not by adding or subtracting the second-harmonic signals obtained with changing the magnetic-field polarity. Whether or not it is eliminated can be judged by comparing the symmetry of signals with respect to the sign reversal of the magnetic field. When an artifact has the same (different) symmetry with that of the SOT-induced Hall signal, it can (cannot) be eliminated.

Figure 7 is for the DLT geometry. For the Hall voltage (V_{xy}) [Fig. 7(a)] not only the SOT signal, but also all other thermoelectric artifacts (T_{x1}, T_{x2}, T_{z1}, and T_{z2}) change their

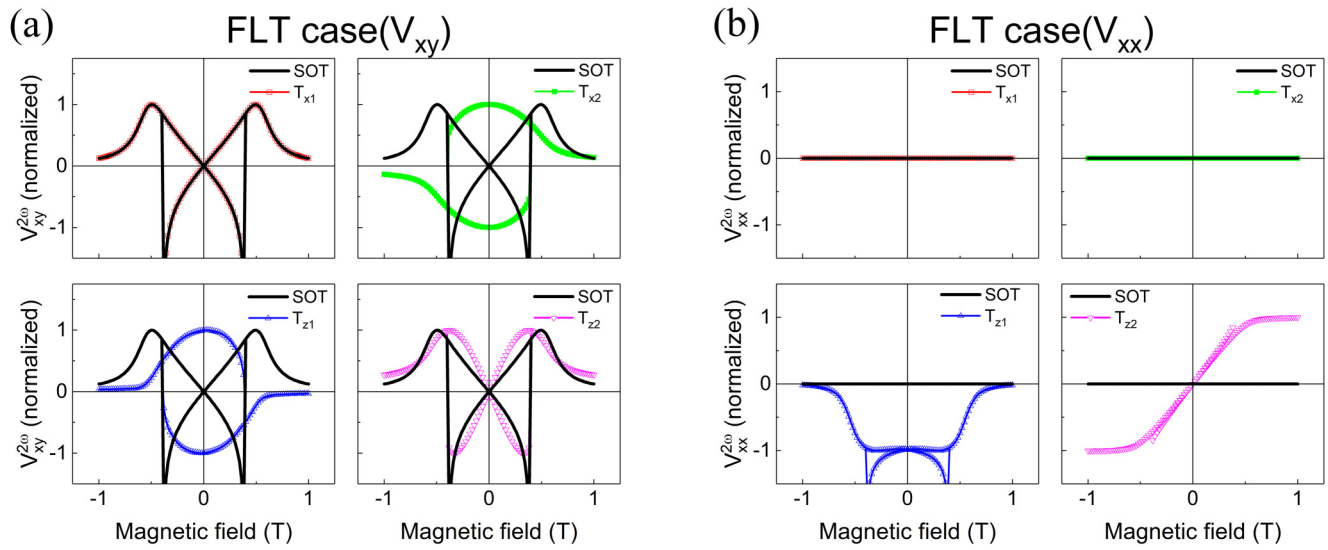

FIG. 8. Macrospin simulation of the second-harmonic signals induced by fieldlike SOT (FLT: black curve) and other thermoelectric effects (red, green, blue, and magenta symbols). (a) Hall voltage (V_{xy}) and (b) longitudinal voltage (V_{xx}), which contaminates Hall signal due to misalignment. T_{ik} means a temperature gradient in the i direction, induced by the kth order of an injected ac current.

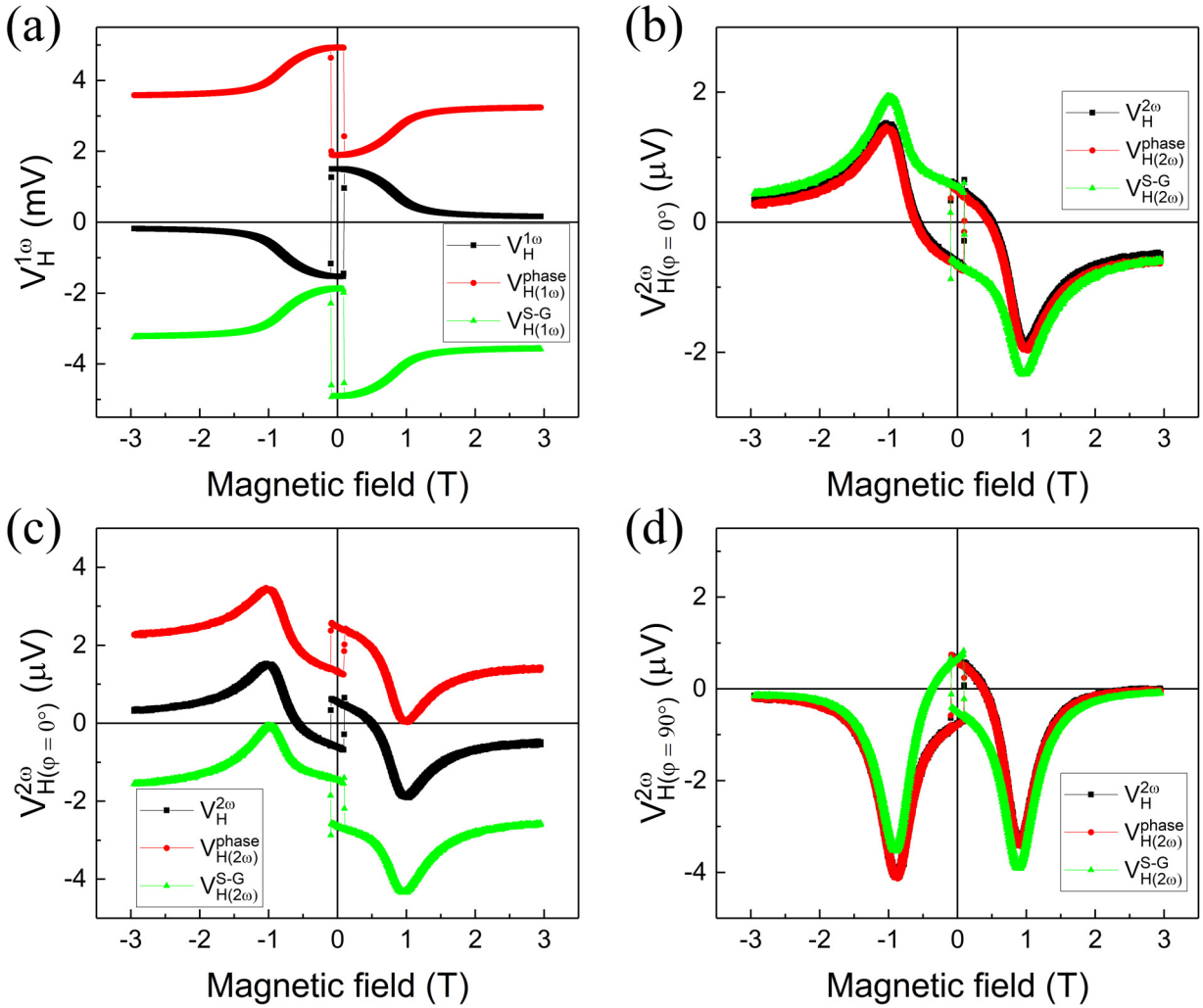

FIG. 9. Comparison of two methods for the change in the polarity of ac current (Ta/CoFeB/MgO). Black symbols (V_H) are the reference data, red symbols (V_H^{phase}) are obtained by changing the phase of the ac current by π, and green symbols (V_H^{S-G}) are obtained by interchanging the source and ground in the current channel. (a) First-harmonic signal with an arbitrary offset. (b) Second-harmonic signal for $\varphi = 0^\circ$ where the offsets are removed. (c) Second-harmonic signal for $\varphi = 0^\circ$ with an arbitrary offset. (d) Second-harmonic signal for $\varphi = 90^\circ$ where the offsets are removed.

signs with respect to the sign reversal of the magnetic field (i.e., all signals are center of symmetric). As a result, no artifact is eliminated by the field-polarity change. For the longitudinal voltage (V_{xx}) [Fig. 7(b)], on the other hand, all SOT and thermoelectric signals are not center of symmetric but mirror symmetric with respect to the magnetic field. Therefore, these artifacts originating from misalignment are completed eliminated by the field-polarity change.

Figure 8 is for the FLT geometry. For the Hall voltage (V_{xy}) [Fig. 8(a)], the SOT signal is mirror symmetric. Among thermoelectric signals, ones due to T_{x1} and T_{z2} are also mirror symmetric so that they are not eliminated by the field-polarity change. However, thermoelectric signals due to T_{x2} and T_{z1} are not mirror symmetric but center of symmetric so that they are eliminated by the field-polarity change. For the longitudinal voltage (V_{xx}) [Fig. 8(b)], only contributions from T_{z1} and T_{z2} could be non-negligible. Using the symmetry comparison, one finds that thermoelectric signals due to $T_{z2}(T_{z1})$ can (cannot) be eliminated by the field-polarity change.

Therefore, when focusing on the field-polarity change, some artifacts (even not all), which are not eliminated in the conventional method, are eliminated by the method proposed in this paper. We note that we consider not only the field-polarity change, but also the current-polarity change in this paper. The latter current-polarity change additionally eliminates artifact(s) as shown in Appendix D. Even though our proposed method cannot eliminate all artifacts due to symmetry, it is still meaningful for SOT studies. The reason is that various artifacts appear in uncontrollable ways and our method eliminates some of them, which was not possible in the conventional method.

APPENDIX D: CHANGE CURRENT POLARITY

To change the polarity of the ac current, we tested two different methods. One is to change the phase of the ac current by π, and the other is to exchange the source and ground of the current channel (i.e., interchanging two current contacts).

If there are no other effects, these two methods must give identical results. However, we found that it is not the case as described below in detail.

Figure 9 shows the first-harmonic signals; $V_H^{1\omega}$ is the reference data, $V_{H,1\omega}^{\text{phase}}$ is obtained by changing the phase of ac current by π, and $V_{H,1\omega}^{S-G}$ is obtained by changing the source and ground of the current channel. Comparing to $V_H^{1\omega}$, the signs of both $V_{H,1\omega}^{\text{phase}}$ and $V_{H,1\omega}^{S-G}$ are reversed as expected. Figure 9(b) shows the second-harmonic signals for the DLT geometry ($H \parallel$ current direction). Figure 9(c) is the same as Fig. 9(b) but with offsets for clarity. We observe that $V_{H,2\omega}^{\text{phase}}$ is identical to $V_H^{2\omega}$, which is caused by the way that the lock-in amplifier reads the second-harmonic signal. For an ac current $I_{\text{ac}} = I_0 \sin(\omega t + \varphi)$, where φ is a phase, the phase-sensitive detector of lock-in amplifier reads the nth harmonic signal as $I_0^n \sin[n(\omega t + \varphi)]$ [42]. Therefore, the second-harmonic signal with $\varphi = \pi$ is $I_0^2[2(\omega + \pi)] - I_0^2 \sin(2\omega t)$, which is identical to the second-harmonic signal with $\varphi = 0$. On the other hand, we observe that $V_{H,2\omega}^{S-G}$ is evidently different from $V_H^{2\omega}$. As the second-harmonic signals originating from SOT must not vary with the current sign, this difference implies that some artifacts contained in $V_H^{2\omega}$ depend on the contracts of current source and ground. Similar trends are also observed for the FLT geometry [H perpendicular to current direction, Fig. 9(d)].

A previously identified artifact in $V_H^{2\omega}$ is caused by the ANE [26], resulting in a hysteresis loop in the second-harmonic signal. We note that this loop reverses its sign in $V_{H,2\omega}^{S-G}$ as compared to $V_H^{2\omega}$ [Fig. 9(c)]. As the ANE corresponding to the hysteresis loop originates from a temperature gradient ∇T_x along the current-flow direction, the sign reversal of hysteresis loop in $V_{H,2\omega}^{S-G}$ means that the sign of ∇T_x also reverses as the contacts of current source and ground are exchanged. We emphasize that this artifact is completely removed by the four-direction method without using the correction suggested in Ref. [26]. This means that the differences between $V_H^{2\omega}$ and $V_{H,2\omega}^{S-G}$, indeed, come from artifacts, which can be eliminated by the four-direction method. This is an example that the current-polarity change additionally eliminates a thermoelectric artifact from the second-harmonic signal.

[1] I. M. Miron, K. Garello, G. Gaudin, P.-J. Zermatten, M. V. Costache, S. Auffret, S. Bandiera, B. Rodmacq, A. Schuhl, and P. Gambardella, Nature (London) **476**, 189 (2011).

[2] L. Q. Liu, C. F. Pai, Y. Li, H. W. Tseng, D. C. Ralph, and R. A. Buhrman, Science **336**, 555 (2012).

[3] S.-W. Lee and K.-J. Lee, Proc. IEEE **104**, 1831 (2016).

[4] G. Yu, P. Upadhyaya, Y. Fan, J. G. Alzate, W. Jiang, K. L. Wong, S. Takei, S. A. Bender, L.-T. Chang, Y. Jiang, M. Lang, J. Tang, Y. Wang, Y. Tserkovnyak, P. K. Amiri, and K. L. Wang, Nat. Nanotechnol. **9**, 548 (2014).

[5] S. Fukami, C. Zhang, S. DuttaGupta, A. Kurenkov, and H. Ohno, Nature Mater. **15**, 535 (2016).

[6] Y.-W. Oh, S.-h.C. Baek, Y. Kim, H. Y. Lee, K.-D. Lee, C.-G. Yang, E.-S. Park, K.-S. Lee, K.-W. Kim, G. Go, J.-R. Jeong, B.-C. Min, H.-W. Lee, K.-J. Lee, and B.-G. Park, Nat. Nanotechnol. **11**, 878 (2016).

[7] A. van den Brink, G. Vermijs, A. Solignac, J. Koo, J. T. Kohlhepp, H. J. Swagten, and B. Koopmans, Nat. Commun. **7**, 10854 (2016).

[8] Y.-C. Lau, D. Betto, K. Rode, J. Coey, and P. Stamenov, Nat. Nanotechnol. **11**, 758 (2016).

[9] K. Cai, M. Yang, H. Ju, S. Wang, Y. Ji, B. Li, K.W. Edmonds, Y. Sheng, B. Zhang, N. Zhang, S. Liu, H. Zheng, and K. Yang, Nature Mater. **16**, 712 (2017).

[10] V. P. Amin and M. D. Stiles, Phys. Rev. B **94**, 104419 (2016); **94**, 104420 (2016).

[11] S.-h.C. Baek, V. P. Amin, Y.-W. Oh, G. Go, S.-J. Lee, G.-H. Lee, K.-J. Kim, M. D. Stiles, B.-G. Park, and K.-J. Lee, Nature Mater. **17**, 509 (2018).

[12] V. P. Amin, J. Zemen, and M. D. Stiles, Phys. Rev. Lett. **121**, 136805 (2018).

[13] A. Thiaville, S. Rohart, É. Jué, V. Cros, and A. Fert, Europhys. Lett. **100**, 57002 (2012).

[14] S. Emori, U. Bauer, S.-M. Ahn, E. Martinez, and G. S. D. Beach, Nat. Mater. **12**, 611 (2013).

[15] K.-S. Ryu, L. Thomas, S.-H. Yang, and S. Parkin, Nat. Nanotechnol. **8**, 527 (2013).

[16] S. A. Siddiqui, J. Han, J. T. Finley, C. A. Ross, and L. Liu, Phys. Rev. Lett. **121**, 057701 (2018).

[17] S. H. Oh and K.-J. Lee, J. Magn. **23**, 196 (2018).

[18] L. Caretta, M. Mann, F. Büttner, K. Ueda, B. Pfau, C. M. Günther, P. Hessing, A. Churikova, C. Klose, M. Schneider, D. Engel, C. Marcus, D. Bono, K. Bagschik, S. Eisebitt, and G. S. D. Beach, Nat. Nanotechnol. **13**, 1154 (2018).

[19] A. Fert, V. Cros, and J. Sampaio, Nat. Nanotechnol. **8**, 152 (2013).

[20] S. Woo, K. Litzius, B. Krüger, M.-Y. Im, L. Caretta, K. Richter, M. Mann, A. Krone, R. M. Reeve, M. Weigand, P. Agrawal, I. Lemesh, M.-A. Mawass, P. Fischer, M. Kläui, and G. S. D. Beach, Nat. Mater. **15**, 501 (2016).

[21] O. Boulle, J. Vogel, H. Yang, S. Pizzini, D. de Souza Chaves, A. Locatelli, T. O. Menteş, A. Sala, L. D. Buda-Prejbeanu, O. Klein, M. Belmeguenai, Y. Roussigné, A. Stashkevich, S. M. Chérif, L. Aballe, M. Foerster, M. Chshiev, S. Auffret, I. M. Miron, and G. Gaudin, Nat. Nanotechnol. **11**, 449 (2016).

[22] Y. Hirata, D.-H. Kim, S. K. Kim, D.-K. Lee, S.-H. Oh, D.-Y. Kim, T. Nishimura, T. Okuno, Y. Futakawa, H. Yoshikawa, A. Tsukamoto, Y. Tserkovnyak, Y. Shiota, T. Moriyama, S.-B. Choe, K.-J. Lee, and T. Ono, Nat. Nanotechnol. **14**, 232 (2019).

[23] L. Liu, T. Moriyama, D. C. Ralph, and R. A. Buhrman, Phys. Rev. Lett. **106**, 036601 (2011).

[24] U. H. Pi, K. W. Kim, J. Y. Bae, S. C. Lee, Y. J. Cho, K. S. Kim, and S. Seo, Appl. Phys. Lett. **97**, 162507 (2010).

[25] J. Kim, J. Sinha, M. Hayashi, M. Yamanouchi, S. Fukami, T. Suzuki, S. Mitani, and H. Ohno, Nat. Mater. **12**, 240 (2013).

[26] K. Garello, I. M. Miron, C. O. Avci, F. Freimuth, Y. Mokrousov, S. Blügel, S. Auffret, O. Boulle, G. Gaudin, and P. Gambardella, Nat. Nanotechnol. **8**, 587 (2013).

[27] M. Hayashi, J. Kim, M. Yamanouchi, and H. Ohno, Phys. Rev. B **89**, 144425 (2014).

[28] S. Emori, E. Martinez, K.-J. Lee, H.-W. Lee, U. Bauer, S.-M. Ahn, P. Agrawal, D. C. Bono, and G. S. D. Beach, Phys. Rev. B **90**, 184427 (2014).

[29] X. Fan, H. Celik, J. Wu, C. Ni, K.-J. Lee, V. O. Lorenz, and J. Q. Xiao, Nat. Commun. **5**, 3042 (2014).

[30] C.-F. Pai, M. Mann, A. J. Tan, and G. S. D. Beach, Phys. Rev. B **93**, 144409 (2016).

[31] J. Park, G. Rowlands, O. Lee, D. C. Ralph, and R. A. Buhrman, Appl. Phys. Lett. **105**, 102404 (2014).

[32] T. Taniguchi, S. Mitani, and M. Hayashi, Phys. Rev. B **92**, 024428 (2015).

[33] W. Legrand, R. Ramaswamy, R. Mishra, and H. Yang, Phys. Rev. Appl. **3**, 064012 (2015).

[34] J. Yoon, S.-W. Lee, J. H. Kwon, J. M. Lee, J. Son, X. Qiu, K.-J. Lee, and H. Yang, Sci. Adv. **3**, e1603099 (2017).

[35] M. M. Decker, M. S. Wörnle, A. Meisinger, M. Vogel, H. S. Körner, G. Y. Shi, C. Song, M. Kronseder, and C. H. Back, Phys. Rev. Lett. **118**, 257201 (2017).

[36] M. Baumgartner, K. Garello, J. Mendil, C. O. Avci, E. Grimaldi, C. Murer, J. Feng, M. Gabureac, C. Stamm, Y. Acremann, S. Finizio, S. Wintz, J. Raabe, and P. Gambardella, Nat. Nanotechnol. **12**, 980 (2017).

[37] J. M. Lee, J. H. Kwon, R. Ramaswamy, J. Yoon, J. Son, X. Qiu, R. Mishra, S. Srivastava, K. Cai, and H. Yang, Commun. Phys. **1**, 2 (2018).

[38] K.-S. Lee, D. Go, A. Manchon, P. M. Haney, M. D. Stiles, H.-W. Lee, and K.-J. Lee, Phys. Rev. B **91**, 144401 (2015).

[39] S.-W. Lee and K.-J. Lee, J. Korean Phys. Soc. **67**, 1848 (2015).

[40] S. J. Yun, E.-S. Park, K.-J. Lee, and S. H. Lim, NPG Asia Mater. **9**, e449 (2017).

[41] O. Lindberg, Proc. IRE **40**, 1414 (1952).

[42] Zurich Instruments, *Principles of Lock-In Detection and the State of the Art* (Zurich Instruments AG, Switzerland, 2016), https://www.zhinst.com/applications/principles-of-lock-in-detection.